A C-terminal PDZ domain-binding sequence is required for striatal distribution of the dopamine transporter

Mattias Rickhag[1,*], Freja Herborg Hansen[1,*], Gunnar Sørensen[1,2], Kristine Nørgaard Strandfelt[1], Bjørn Andresen[1], Kamil Gotfryd[1], Kenneth L. Madsen[1], Ib Vestergaard Klewe[1], Ina Ammendrup-Johnsen[1], Jacob Eriksen[1], Amy H. Newman[3], Ernst-Martin Füchtbauer[4], Jesus Gomeza[5], David P.D. Woldbye[2], Gitta Wörtwein[2,6] & Ulrik Gether[1]

The dopamine transporter mediates reuptake of dopamine from the synaptic cleft. The cellular mechanisms controlling dopamine transporter levels in striatal nerve terminals remain poorly understood. The dopamine transporters contain a C-terminal PDZ (PSD-95/Discs-large/ZO-1) domain-binding sequence believed to bind synaptic scaffolding proteins, but its functional significance is uncertain. Here we demonstrate that two different dopamine transporter knock-in mice with disrupted PDZ-binding motifs (dopamine transporter-AAA and dopamine transporter + Ala) are characterized by dramatic loss of dopamine transporter expression in the striatum, causing hyperlocomotion and attenuated response to amphetamine. In cultured dopaminergic neurons and striatal slices from dopamine transporter-AAA mice, we find markedly reduced dopamine transporter surface levels and evidence for enhanced constitutive internalization. In dopamine transporter-AAA neurons, but not in wild-type neurons, surface levels are rescued in part by expression of a dominant-negative dynamin mutation (K44A). Our findings suggest that PDZ-domain interactions are critical for synaptic distribution of dopamine transporter *in vivo* and thereby for proper maintenance of dopamine homoeostasis.

[1] Molecular Neuropharmacology Laboratory, Lundbeck Foundation Center for Biomembranes in Nanomedicine, Department of Neuroscience and Pharmacology, Faculty of Health and Medical Sciences, University of Copenhagen, Copenhagen, Denmark. [2] Laboratory of Neuropsychiatry, Department of Neuroscience and Pharmacology, Faculty of Health and Medical Sciences, University of Copenhagen, Copenhagen, Denmark. [3] National Institute on Drug Abuse-Intramural Research Program, National Institutes of Health, Baltimore, Maryland 21224, USA. [4] Department of Molecular Biology, Aarhus University, Aarhus, Denmark. [5] Institute for Pharmaceutical Biology, University of Bonn, Bonn, Germany. [6] Department of Public Health, Faculty of Health and Medical Sciences, University of Copenhagen, Copenhagen, Denmark. * These authors contributed equally to this work. Correspondence and requests for materials should be addressed to U.G. (email: gether@sund.ku.dk).

opamine has an important role in modulating motor activity, cognition, neuroendocrine functions and reward mechanisms. Aberrant dopaminergic signalling is involved in several CNS disorders, including schizophrenia, attention-deficit hyperactivity disorder, drug addiction and Parkinson's disease[1–3]. The presynaptic dopamine transporter (DAT), is responsible for sequestering released dopamine from the synaptic cleft[3]. Moreover, the transporter represents the major target for psychostimulants, such as cocaine and amphetamine[4]. Characterization of mice with genetic deletion of DAT expression (DAT KO) has demonstrated that DAT is fundamental for spatio-temporal regulation of synaptic dopamine. DAT KO mice exhibit a hyperdopaminergic state with prolonged dopamine clearance and profound alterations of extracellular dopamine dynamics[5]. The behavioural manifestations in DAT KO mice include locomotor hyperactivity, endocrine deficits and impaired psychostimulant response[5,6].

It remains unresolved how dopaminergic neurons ensure proper DAT levels in the plasma membrane of the presynaptic dopaminergic terminals. Recent efforts have identified several DAT-associated proteins, consistent with DAT being part of a multi-protein network responsible for controlling the subcellular distribution of DAT[7]. Interestingly, DAT contains, at its extreme C-terminus, a PDZ (PSD-95/Discs-large/ZO-1) homology-binding sequence, shown to bind the PDZ domain of PICK1 (protein interacting with C kinase 1)[8]. PDZ domains are modular protein–protein interaction domains found in scaffolding proteins and known to have key roles in assembly of large multi-protein complexes, as well as in regulating trafficking of binding partners[9–11]. The interaction between PICK1 and DAT was originally proposed to be important for endoplasmic reticulum (ER) export of DAT, because C-terminal truncations of DAT resulted in ER retention and impaired surface expression of DAT in heterologous cell lines[12]. However, we later demonstrated that the PDZ-binding sequence of DAT is neither necessary nor sufficient for DAT surface expression in heterologous cells[13]. Thus, the cellular and physiological importance of DAT PDZ domain interactions *in vivo* has remained unclear.

Here, we investigate the significance of the C-terminal PDZ domain-binding sequence for DAT function *in vivo* by generating DAT knock-in mice with disrupted PDZ domain-binding sequences. To disrupt any possible PDZ domain interactions, we first substitute the PDZ-target sequence (–LLV) with alanine residues (DAT-AAA). The disruption has major consequences for distribution of the transporter with 80–90% decrease in transporter levels in striatal terminals of dopaminergic neurons, without interfering with folding and ER export of the transporter. In agreement with unique alterations in dopaminergic signalling, this change in DAT distribution causes significant behavioural changes and attenuated amphetamine sensitivity. Further support for an indispensable role of the PDZ-binding sequence for striatal DAT distribution is obtained in a second DAT knock-in mouse in which PDZ domain interactions are disrupted through addition of a single C-terminal alanine (DAT + Ala). Remarkably, corresponding changes in DAT distribution are not observed in PICK1 knock-out mice supporting that PICK1 is not critical for synaptic DAT distribution *in vivo*.

Results

Mutation of the DAT C-terminal PDZ-binding sequence. The human DAT contains a C-terminal PDZ-binding sequence (− LKV) that previously was shown by other investigators and by us to interact with the PDZ domain of PICK1[8,13,14]. Upon alanine substitution of the last three C-terminal residues in human DAT (618–620), the interaction was disrupted[13]. Using a fluorescent polarization assay, we found that the mouse DAT C-terminus (–LLV) also binds to the PICK1 PDZ domain (Fig. 1a,b)[14], and that alanine substitution of the PDZ-binding sequence in mouse DAT markedly decreased the binding affinity (WT: $K_i = 0.68\,\mu M$; DAT-AAA: $K_i = 20.1\,\mu M$) (Fig. 1b).

Reduction in striatal distribution of DAT in DAT-AAA mice. To assess the significance of PDZ domain interactions for DAT function *in vivo*, we generated a DAT knock-in mouse strain expressing the DAT-AAA mutant instead of WT (Supplementary Fig. S1). Introduction of DAT-AAA did not affect transcription of the DAT gene, that is, similar mRNA levels were found in DAT-AAA mice and WT littermates. The mRNA levels for tyrosine hydroxylase (TH), a key enzyme in dopamine synthesis, and marker of dopaminergic neurons, were also similar in WT and DAT-AAA mice (Fig. 1c).

The cellular distribution of DAT-AAA was assessed by immunohistochemical characterization. DAT-immunoreactivity (DAT-ir) was localized predominantly to the dorsal/ventral striatum, olfactory tubercles and midbrain (substantia nigra (SN) and ventral tegmental area (VTA)) (Fig. 1d,e), confirming previous reports[15,16]. As expected, we observed strong DAT-ir of axonal terminals in striatum of WT mice, whereas DAT-AAA mice displayed a remarkable loss of DAT-ir. In contrast, immunolabelling of TH demonstrated dense staining of axonal fibres in striatum with similar intensities in both genotypes (Fig. 1d).

In the ventral midbrain, DAT-ir was observed in perikarya and extensions of both WT and DAT-AAA mice; however, as in striatum, DAT-AAA mice showed decreased density in SN and VTA, particularly corresponding to the dendrites (Fig. 1e). TH immunolabeling showed once again intense labelling of perikarya and processes in both genotypes (Fig. 1e). Strikingly, quantification of immunoreactivity showed that DAT-ir in striatum from DAT-AAA mice was reduced to ∼30% of WT, while SN and VTA showed a less pronounced decrease (SN ∼81% and VTA 76% of WT) (Fig. 1f). The massive loss of DAT-ir fibres in DAT-AAA mice was emphasized in a sagittal view, showing midbrain projections radiating into the terminal fields of striatum (Supplementary Fig. S1). Quantification of TH-ir showed no significant difference between genotypes (Fig. 1f).

Immunoblotting of striatal membrane preparations confirmed that DAT levels in DAT-AAA mice were dramatically reduced, whereas total TH protein was practically unaltered (Fig. 2a). The level of functional DAT in striatal membranes was investigated in radioligand-binding experiments using the DAT ligand [125I]-RTI-55. The number of maximal binding sites (B_{max}) was reduced to ∼10% of WT without change in affinity (Fig. 2b). We also performed autoradiography using the DAT ligand, [3H]-mazindol. Whereas WT mice had a considerable density of DAT-binding sites in both striatum and midbrain, [3H]-mazindol binding was apparently absent in both striatum and midbrain of DAT-AAA mice (Fig. 2c,d). Note that the sensitivity of [3H]-mazindol autoradiography conceivably is lower than that of [125I]-RTI-55 binding. This may explain the absence of [3H]-mazindol binding in DAT-AAA mice. Levels of functional DAT in striatum were also addressed by evaluating [3H]-dopamine uptake in striatal synaptosomes. DAT-AAA mice displayed extensive, but not complete, loss of uptake capacity (Fig. 2e). Finally, we quantified the amount of surface-expressed transporters by surface biotinylation in striatal slices, where DAT-AAA levels were reduced to ∼8% of WT levels (Fig. 2f).
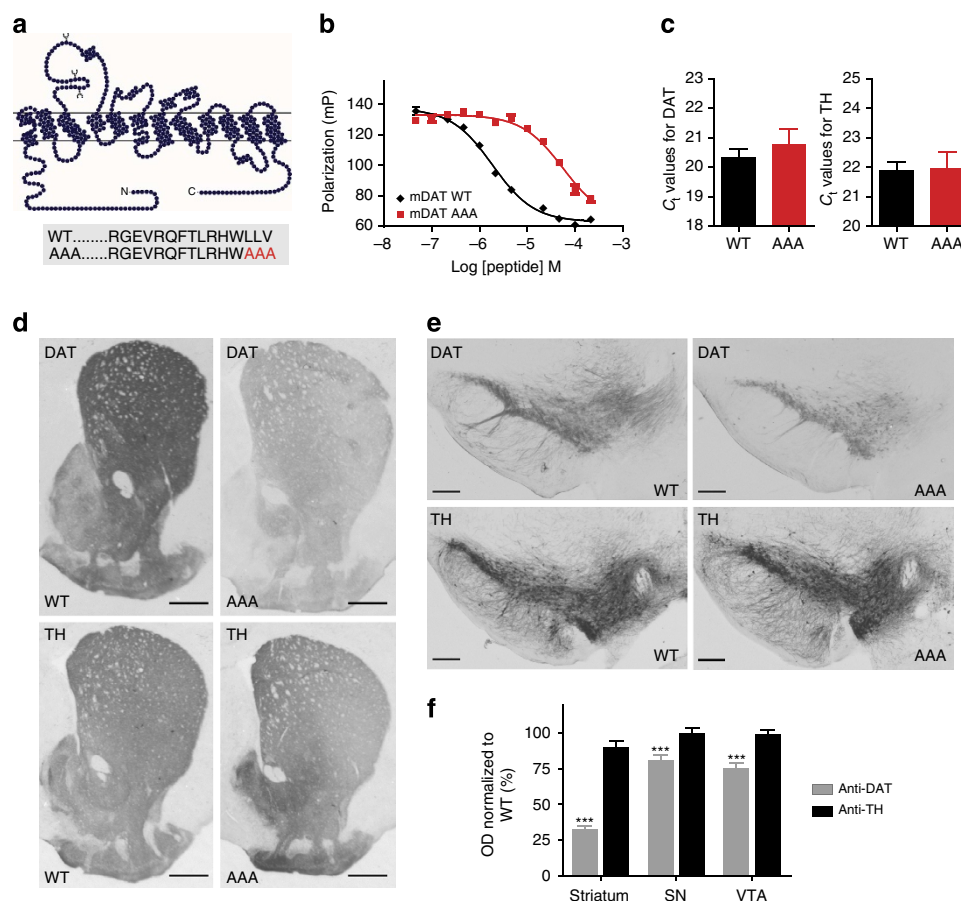
Figure 1 | Immunohistochemical characterization of DAT-AAA mice with disrupted C-terminal PDZ-target sequence. (**a**) Schematic representation of mDAT topology and C-terminal sequences for WT DAT and DAT-AAA with alanine substitution of three C-terminal residues. (**b**) Fluorescence polarization competition binding assay on purified PICK1 using 40 nM Oregon Green-labelled human DAT peptide (13 C-terminal residues) and increasing concentration of indicated unlabelled peptides (equivalent to the 13 C-terminal residues of mDAT WT and DAT-AAA). Data are polarization values (mP) (means ± s.e.m., $n = 3$). (**c**) Quantitative real-time PCR of midbrain tissue from WT and DAT-AAA mice demonstrates no difference in mRNA expression levels. Data are shown as raw cycle threshold (C_t) values for DAT and TH (means ± s.e.m., $n = 4$, non-parametric Mann–Whitney test, $P > 0.05$). (**d,e**) Representative photomicrographs of DAT-ir and TH-ir in striatum (scale bar = 500 μm) and midbrain (scale bar = 200 μm) from WT and DAT-AAA mice. A substantial loss of DAT-ir is observed in DAT-AAA mice, while TH-ir displays similar intensities in both genotypes. (**f**) Optical densitometry was applied for semi-quantification of DAT and TH levels. Mean values were calculated and values from knock-in mice were normalized to WT (means ± s.e.m., Str = 33%, SN = 81% and VTA = 76% of WT, ***$P < 0.001$, $n = 5$, one-way analysis of variance with *post-hoc* Bonferroni's multiple comparison test).

In summary, our data demonstrate a pronounced reduction in the striatal levels of DAT in DAT-AAA mice, without altered activity of the transporters present.

Extensive loss of DAT in synaptic terminals from DAT-AAA. Confocal imaging of striatal sections from WT mice showed an extensive network of DAT-labelled axonal terminals in striatum with a punctate pattern, except in areas where white matter bundled and neuronal perikarya intervened (Fig. 3). Imaging of striatal sections from DAT-AAA mice revealed a prominent loss of DAT-labelled axonal terminals. In contrast, the pattern of TH labelling was similar in WT and DAT-AAA mice, demonstrating intense staining of terminals with a punctate labelling pattern of filaments partially overlapping with DAT (Fig. 3a,b). DAT-ir in SN from DAT-AAA mice was predominantly localized to perikarya where the intensity was similar to that seen in WT. The neuronal processes, however, showed scarce labelling in DAT-AAA mice, while detailed micrographs from WT mice demonstrated a ramified, complex network of dendrites. Immunofluorescent TH labelling of WT midbrain neurons showed

substantial overlay with DAT, and DAT-AAA mice showed a similar pattern of TH-ir as WT mice (Fig. 3c,d).

Altered behaviour of DAT-AAA mice. Behavioural and physical characteristics of experimentally naive mice were assessed using the SHIRPA primary screen procedure, which comprises several measures covering various reflexes and basic sensorimotor functions (Supplementary Table S1)[17]. To reveal specific behavioural consequences of the mutation, we tested basal locomotion and amphetamine-induced hyperactivity. During the first 90 min of the 4-h test session, DAT-AAA mice were hyperactive, compared with WT mice (Fig. 4a). Hyperactivity was also observed after saline injection (Fig. 4b). As expected, WT mice responded with significant hyperactivity upon treatment with i.p. amphetamine (1, 2 or 3 mg kg^{-1}), whereas DAT-AAA mice exhibited an attenuated amphetamine response with no significant change in locomotor activity (Fig. 4b). We also tested the effect of 2 mg kg^{-1} i.p. amphetamine in the DAT-AAA mice after 2.5 h of habituation in the activity boxes. Once again there was no significant effect of amphetamine in the DAT-AAA mice,
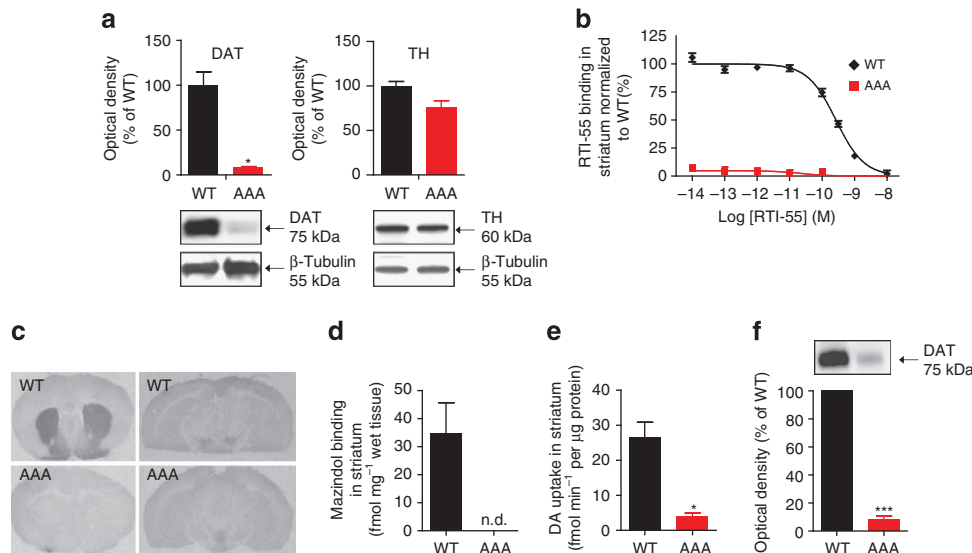
Figure 2 | Assessment of DAT-binding sites and dopamine transport in DAT-AAA mice. (**a**) Immunoblotting confirmed a major loss of DAT expression in striatum, while TH levels were similar to WT. Upper panels, densitometric analysis of immunoblots for WT and DAT-AAA mice, *$P < 0.05$, non-parametric Mann–Whitney test (means ± s.e.m., $n = 4$). Lower panels, representative immunoblots for DAT (left) and TH (right) in striatal lysates from WT and DAT-AAA mice. (**b**) Competition binding experiments on striatal membranes using the high-affinity DAT ligand [^{125}I]-RTI-55. Data are normalized to WT littermate controls ($n = 4$). [^{125}I]-RTI-55 binding was analysed by non-linear regression analysis using GraphPad Prism 5.0. The affinity constants (K_i) were determined assuming one-site binding. B_{max} and K_d values were obtained from the half-maximal inhibitory concentration (IC50) value estimated by assuming a sigmoidal one-site curve (One site – Fit LogIC50). B_{max}: WT, 290 ± 50 fmol per µg protein; DAT-AAA, 30 ± 6.2 fmol per µg protein (means ± s.e.m., $n = 4$); K_d: WT, 0.127 (0.105–0.154) nM; DAT-AAA, 0.334 (0.108–1.062) nM (means (s.e.m. interval), $n = 4$). (**c,d**) [^{3}H]-mazindol autoradiography shows a high density of DAT-binding sites in striatum from WT mice, while binding is absent in DAT-AAA mice (means ± s.e.m., $n = 4$). Midbrain region shows lower density of binding sites in WT and binding is practically absent in DAT-AAA mice. (**e**) Extensive loss of [^{3}H]-dopamine uptake (0.125 µM) in striatal synaptosomes from DAT-AAA mice relative to WT, *$P < 0.05$, non-parametric Mann–Whitney test (means ± s.e.m., $n = 4$–5). (**f**) Surface biotinylation of striatal slices show a dramatic loss of surface-expressed DAT in DAT-AAA mice (% of WT control ± s.e.m., one-sample t-test, $n = 3$, ***$P < 0.001$).

whereas the 2 mg kg^{-1} dose increased activity in WT (Fig. 4c). Consistent with the findings in activity boxes, DAT-AAA mice showed increased locomotor activity in an open-field test, assessed as total distance moved (Fig. 4d).

DAT-AAA surface expression is reduced in dopaminergic neurons. To investigate the cellular phenotype of DAT-AAA, we prepared postnatal midbrain cultures of dopaminergic neurons. Immunostainings of WT neurons demonstrated widespread distribution of DAT-ir in neuronal extensions, varicosities and perikarya (Fig. 5a). The immunosignal was prominently reduced in DAT-AAA neurons and appeared more localized to the somas (Fig. 5a), consistent with the DAT staining pattern observed in DAT-AAA midbrain sections (Fig. 3c). However, some DAT-ir was clearly present in the neuronal extensions as well.

To visualize surface-expressed DAT, we exploited our recently developed fluorescent cocaine analogue, JHC 1–64, permitting labelling of correctly folded transporter in the plasma membrane of live neurons[18]. As previously reported for rat neurons[18], we observed a specific fluorescent signal in WT neurons from mice, with uniform distribution in the plasma membrane of perikarya and extensions (Fig. 5b). Labelling of DAT-AAA-derived neurons revealed less staining intensity, consistent with a substantial reduction in surface expression of DAT-AAA.

Next, we performed immunoblotting experiments on cell lysates from the dopaminergic neurons, as well as from whole brain membrane fractions of WT and DAT-AAA pups (P1–P3). In whole brain lysates, both WT DAT and DAT-AAA eluted as a single ∼70-kDa band with no detection of smaller, immature glycoforms (Fig. 5c). Similar results were obtained from whole

brain membranes in adult WT and DAT-AAA mice (data not shown). The substantially lowered intensity of the DAT-AAA band confirmed that DAT-AAA levels are strongly reduced already at postnatal day 1–3 (Fig. 5c). The transporter also eluted as a single ∼70 kDa band in lysates from the cultured neurons, equivalent to full-length, glycosylated DAT (Fig. 5d). To validate that this DAT band corresponded to mature, fully glycosylated DAT, we treated the neuronal lysates with endoglycosidase H (Endo H) or peptide N-glycosidase F (PNGase F). Endo H selectively cleaves ER glycoforms of glycoproteins, while PNGase F cleaves all asparagine-linked oligosaccharides. Endo H treatment had no effect, suggesting that the detectable DAT has trafficked beyond ER (Fig. 5d and Supplementary Fig. S2 for positive Endo H control). In contrast and in agreement with mature glycosylation, PNGase F treatment removed the 70-kDa band and gave instead rise to a band of ∼45 kDa, most likely corresponding to a completely deglycosylated transporter (Fig. 5d).

Elution of DAT as a single, mature band argues against simple ER retention causing impaired synaptic distribution of DAT-AAA. To exclude the possibility that immaturely ER-retained DAT-AAA might be subject to rapid proteosomal degradation that prevents detection of the immature forms, neuronal cultures were treated with a proteosomal inhibitor, MG-132. This treatment did not give rise to detectable immature non-glycosylated bands (Supplementary Fig. S2). Additional experiments in transfected heterologous cells argued further against ER retention of DAT-AAA. Upon transfection of both HEK293 cells and N2A cells, we observed equivalent [^{3}H]-dopamine uptake capacity (V_{max}) for both WT and DAT-AAA, with no obvious difference in K_m values
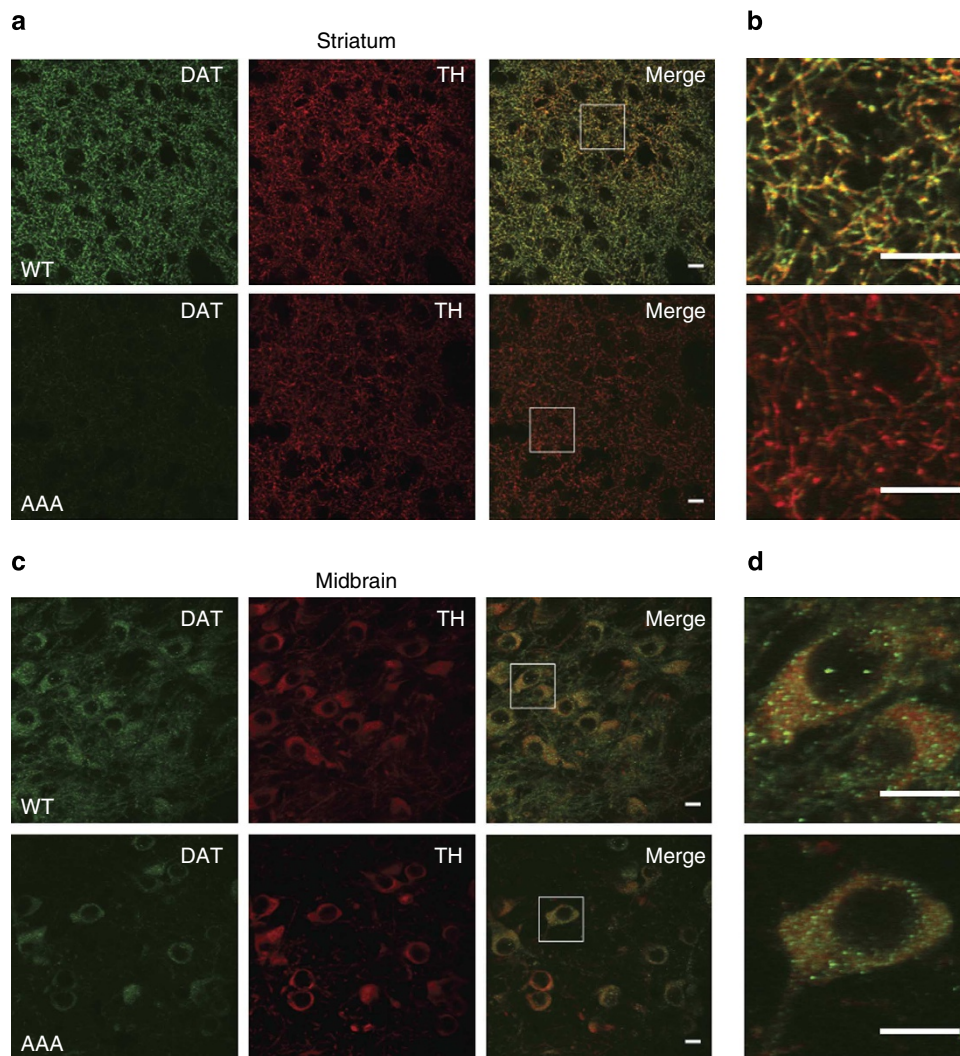
Figure 3 | Presynaptic terminals in striatum from DAT-AAA mice demonstrate substantial loss of DAT expression. (**a**) Axonal terminals in striatum labelled for DAT (green, Alexa-488) show dense DAT-ir in WT mice, while DAT-AAA mice display almost a complete loss of DAT-ir. Co-localization with TH (red, Alexa-568) demonstrates partial overlay in both WT and DAT-AAA mice. TH distribution demonstrates similar intensities in both genotypes with a typical punctate pattern. (**b**) Higher magnification images from WT mice show a typical punctate DAT labelling of presynaptic terminals in striatum, while scarce distribution is observed in DAT-AAA mice. (**c**) Neuronal cell bodies in SN from WT mice display intense DAT-ir in both cell soma and extensions, while labelling in DAT-AAA mice is confined mainly to the cell soma region. TH-ir shows prominent labelling of midbrain neurons in both WT and DAT-AAA mice. (**d**) Higher magnification images from midbrain of WT and DAT-AAA. All scale bars, 10 μm.

(Supplementary Fig. S3). This agrees with our previous observations in human DAT-AAA[13] and is in contrast to the effect of C-terminal truncations, which are known to cause ER retention[8,12,13,19]. Of notice, this suggests that the importance of the C-terminal PDZ-binding sequence cannot be reproduced in heterologous expression systems. Altogether, we conclude that the loss of DAT-AAA in synaptic terminals is unlikely to be a consequence of misfolding and ER retention.

Increased internalization of DAT-AAA in dopaminergic neurons. A possible explanation for the dramatic loss of striatal DAT in DAT-AAA mice is a decrease in DAT-AAA surface stability leading to enhanced internalization and lysosomal degradation. Constitutive DAT internalization has been demonstrated in both transfected heterologous cells and dopaminergic neurons[20–22]. To assess constitutive internalization, we used the fluorescent cocaine analogue, JHC 1–64, which does not influence

DAT trafficking and has a very slow off-rate, which makes it suitable for studying DAT internalization[18]. Surface-expressed DAT was labelled with JHC 1–64 at 4 °C, followed by 1 h internalization at 37 °C. Internalized, JHC 1–64-labelled DAT was visible as distinct intracellular vesicular structures in both DAT-AAA and WT neurons. These structures were not observed in 4 °C controls (Fig. 6a). The internalization was clearly seen corresponding to the somas and their proximal extensions, although more difficult to identify in the distal thin extensions. Interestingly, the constitutive internalization appeared intense in many of the DAT-AAA neurons compared with the low intensity of the surface labelling. Accordingly, we quantified the internalized fraction and confirmed that a significantly larger fraction of DAT-AAA was internalized compared with WT DAT (Fig. 6b). We showed previously that constitutively internalized WT preferentially sorts to lysosomes in rat dopaminergic neurons[23]. To investigate the fate of internalized DAT-AAA, we visualized internalized JHC 1–64-labelled DAT in the presence
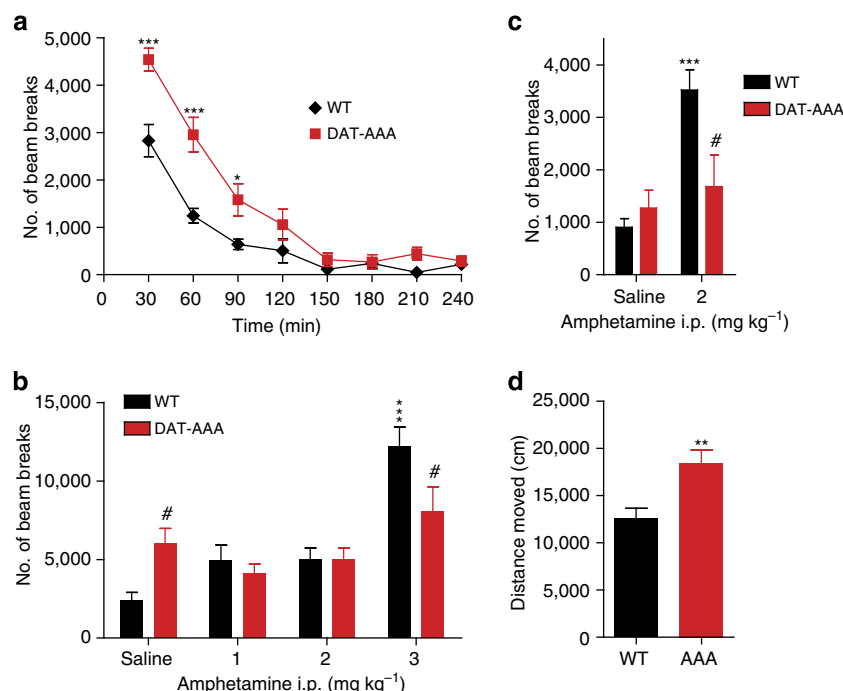
Figure 4 | Basal and amphetamine-induced locomotion. (a) Four hours basal locomotion. Mice were placed in an activity box and locomotion was measured as total beam breaks in 30 min bins. Data are means ± s.e.m., *$P < 0.05$, ***$P < 0.001$, Bonferroni *post-hoc* t-tests after significance in a two-way analysis of variance (ANOVA), $F(7,175) = 7.5$; $P < 0.001$; $n_{WT} = 14$, $n_{AAA} = 13$. **(b)** Amphetamine-induced hyperactivity. Locomotion was evaluated as total beam breaks during 1 h. Data are means ± s.e.m., #$P < 0.05$, versus corresponding WT, Bonferroni *post-hoc* t-tests after significant two-way ANOVA, $F(3,91) = 5.58$; $P < 0.01$. ***$P < 0.001$ versus own saline group after significant one-way ANOVA; WT ($F(3,26) = 23.5$; $P < 0.001$); $n_{WT} = 7-9$, $n_{AAA} = 9-10$. **(c)** Amphetamine-induced hyperactivity after habituation. Locomotor activity is presented as total beam breaks during 2.5 h (means ± s.e.m), #$P < 0.05$ versus corresponding WT, Bonferroni *post-hoc* t-tests after significant two-way ANOVA, $F(1,27) = 11.12$; $P < 0.01$. ***$P < 0.001$ versus own saline group, Student's t-test versus WT/saline, $t(11) = 5.88$, $n_{WT} = 6-7$, $n_{AAA} = 9$. **(d)** Basal locomotion in open-field during 30 min. Mice were placed in the centre of an open field and locomotion was measured as total distance moved. Data are means ± s.e.m., **$P < 0.01$, $t(19) = 3.4$; $n_{WT} = 11$, $n_{AAA} = 10$.
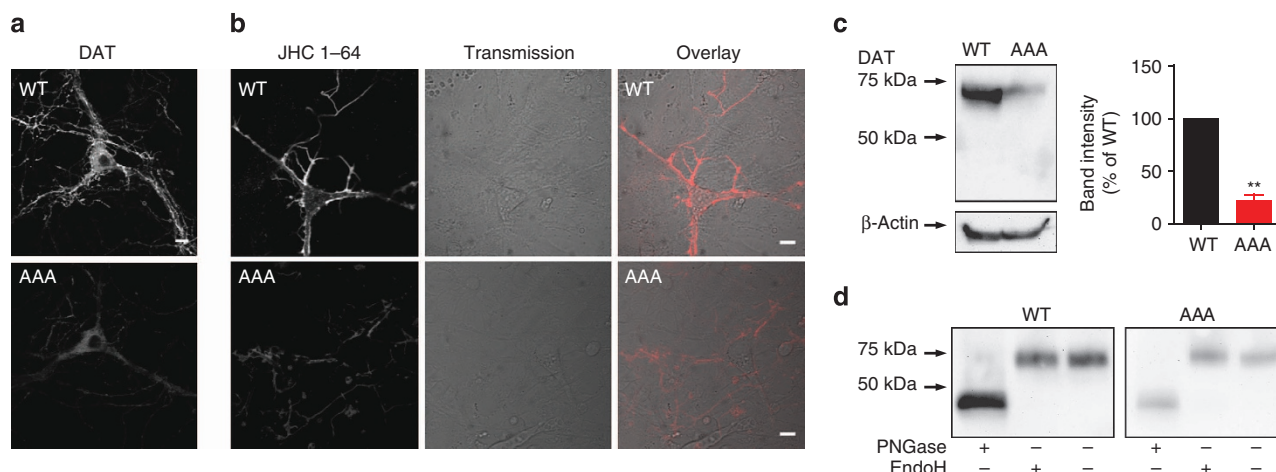

Figure 5 | Dopaminergic neurons show reduced DAT-AAA surface expression and no ER retention of DAT-AAA. (a) Visualization of DAT in dopaminergic neurons from WT and DAT-AAA mice by immunostaining and confocal microscopy. DAT-AAA labelling intensity was dramatically reduced compared with WTDAT. Labelling was most intense in somas, but DAT-AAA was clearly present in extensions as well. Images are representative stainings of three independently prepared cultures. **(b)** Confocal live imaging of midbrain neurons derived from WT or DAT-AAA mice. Neurons were stained with the fluorescent cocaine analogue, JHC 1–64 (10 nM), to obtain specific labelling of endogenously expressed WT and DAT-AAA present in the plasma membrane. Neurons from DAT-AAA mice exhibited markedly reduced surface labelling. Pictures are representative for three independently prepared cultures. Scale bars, 10 μm. **(c)** Immunoblotting of membrane fractions derived from whole brains of new born pups (P1–P3). Left panel, representative immunoblot. A single DAT band (~70 kDa) is detected in membrane fractions from both WT and DAT-AAA pups, albeit with markedly reduced intensity for DAT-AAA. Note that no immature DAT bands were detected in either genotype. Right panel, densitometric analysis of immunoblots shown as % of WT, means ± s.e.m., **$P < 0.01$, one-sample t-test. **(d)** Endo H and PNGase F treatment of neuronal lysates. Immunoblotting of lysates from cultured dopaminergic neurons likewise show that untreated lysates give rise to a single DAT band (~70 kDa), for both WT and DAT-AAA, with no detectable immature bands. Both the WT and the DAT-AAA bands are insensitive to Endo H treatment, but elutes at ~45 kDa after deglycosylation by PNGase F ($n = 3$).
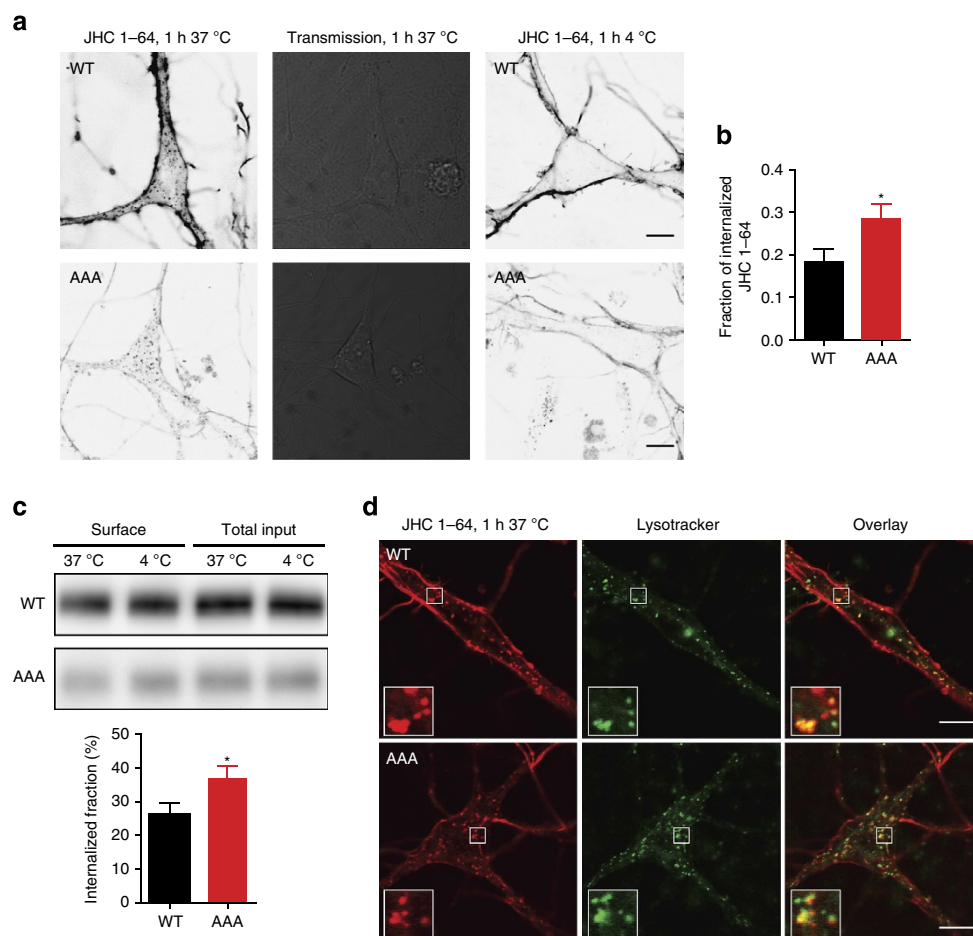
Figure 6 | Visualization of constitutive DAT internalization in WT and DAT-AAA neurons. (**a**) Visualization of constitutive internalization of DAT in WT and DAT-AAA neurons by confocal live imaging using the fluorescent cocaine analogue, JHC 1–64. Left panels, surface-expressed DAT was labelled by incubation of neurons with 10 nM JHC 1–64 at 4 °C, followed by 1 h incubation at 37 °C to allow internalization. Middle panels, transmission image. Right panels, 4 °C temperature control for internalization. Fluorescence is shown on a grey scale with the highest fluorescence represented by the darkest pixels. Internalization of DAT/JHC 1–64 complexes is seen as JHC 1–64-positive vesicular structures in the neuronal soma and proximal extensions. Similar JHC 1–64-positive vesicles did not appear under 4 °C control conditions. Images shown were taken with identical settings to visualize the JHC 1–64 intensity under identical conditions for WT and DAT-AAA neurons. (**b**) Quantification of internalized DAT. The amount of internalized DAT was quantified relative to the total amount of JHC 1–64-labelled DAT and showed that a significantly larger fraction of DAT was internalized in DAT-AAA neurons ($n = 20$ neurons) compared with WT neurons ($n = 30$ neurons), means ± s.e.m., *$P < 0.05$, non-parametric Mann–Whitney test. (**c**) Surface biotinylation of striatal slices. Striatal slices were biotinylated after 1 h incubation at either 37 °C to allow internalization, or at 4 °C, a non-trafficking temperature control. Upper and middle panels, representative blots of WT and DAT-AAA lysates, respectively. Lysates from DAT-AAA and WT mice were run on separate gels to allow better visualization of the DAT-AAA band without reaching saturating levels of the WT band intensity. Lower panel, quantification of internalized fractions, that is, the reduction in surface levels. The internalized fraction was significantly larger in DAT-AAA slices, means ± s.e.m, *$P < 0.05$, one-tailed t-test, $n = 3$. (**d**) Co-localization between constitutively internalized JHC 1–64/DAT complexes and LysoTracker. A considerable amount of co-localization with LysoTracker is seen for both WT DAT and DAT-AAA. Scale bars, 10 µm.

of the lysosomal marker, LysoTracker. Both internalized DAT-AAA and WTDAT displayed considerable co-localization with LysoTracker, indicating that also the majority of internalized DAT-AAA most likely is sorted to degradation (Fig. 6d).

To obtain further support for enhanced internalization of DAT-AAA, we rationalized that in striatal slices, striatal dopaminergic terminals would be disconnected from the somas and thereby from continuous supply of newly synthesized DAT. In turn, this should allow us to detect a putative reduction in DAT surface levels resulting from constitutive redistribution of the transporter away from the surface. Indeed, as assessed by a surface biotinylation protocol, a decrease in both WT and DAT-AAA surface levels could be detected in the slices after 1 h incubation at 37 °C compared with incubation at a trafficking non-permissive temperature (4 °C control) (Fig. 6c). Importantly,

the reduction (indicated as internalized fraction) was relatively larger in DAT-AAA striatal slices (Fig. 6c), consistent with our findings in cultured neurons. Thus, DAT-AAA exhibits a larger redistribution to cytosolic compartments during conditions where supply of transporter to the surface is limited to the intracellular pool, present in terminals at the beginning of the experiment.

Inhibiting endocytosis rescues DAT-AAA surface expression. We hypothesized that if DAT-AAA undergoes accelerated endocytosis, inhibiting this constitutive endocytosis should rescue DAT-AAA surface levels. Constitutive DAT internalization has been shown to be clathrin/dynamin-dependent[18,20]. Therefore, we inhibited endocytosis using the dominant-negative dynamin mutant, K44A, previously shown to reduce DAT

internalization[18,24]. WT or K44A dynamin were expressed in dopaminergic neurons, using recombinant lentiviral vectors, and transduced neurons were identified by concurrent expression of enhanced green fluorescent protein (EGFP). Although the transduction efficiency was high, only few transduced dopaminergic neurons could be identified, underlining the general difficulties in achieving heterologous expression in these neurons. Nonetheless, careful live confocal imaging, following labelling with the cocaine analogue JHC 1–64 to assess transporter surface levels, permitted identification of several transduced dopaminergic neurons. The imaging analysis suggested increased JHC 1–64 surface signal in K44A-transduced DAT-AAA neurons compared with WT dynamin-transduced neurons (Fig. 7a–d). This was confirmed by quantification of the surface signal by calculating the mean intensity of JHC 1–64 labelling of soma and proximal extensions relative to control neurons. This revealed a significant increase in the relative surface signal of DAT-AAA in K44A-expressing

neurons, whereas no detectable effect of K44A was seen in WT neurons (Fig. 7a–d).

DAT-AAA and DAT + Ala phenotypes are not dependent on PICK1. DAT and TH immunoreactivity was also investigated in an additional DAT knock-in strain, DAT + Ala, where addition of an alanine to the C-terminus disrupted interactions with PDZ domain proteins (Supplementary Fig. S4). DAT + Ala mice demonstrated a similar, though less pronounced, decrease in striatal DAT-ir concomitant with reduced labelling of neuronal processes in midbrain. TH-ir showed similar intensities in dopaminergic areas from WT and DAT + Ala mice. Immuno-blotting confirmed reduced DAT levels in striatum of DAT + Ala mice (Fig. 8a–d). To determine if DAT + Ala mice exhibit a similar behavioural phenotype as DAT-AAA mice, basal locomotor activity was investigated in an open-field test. Indeed, DAT + Ala mice showed increased basal locomotion
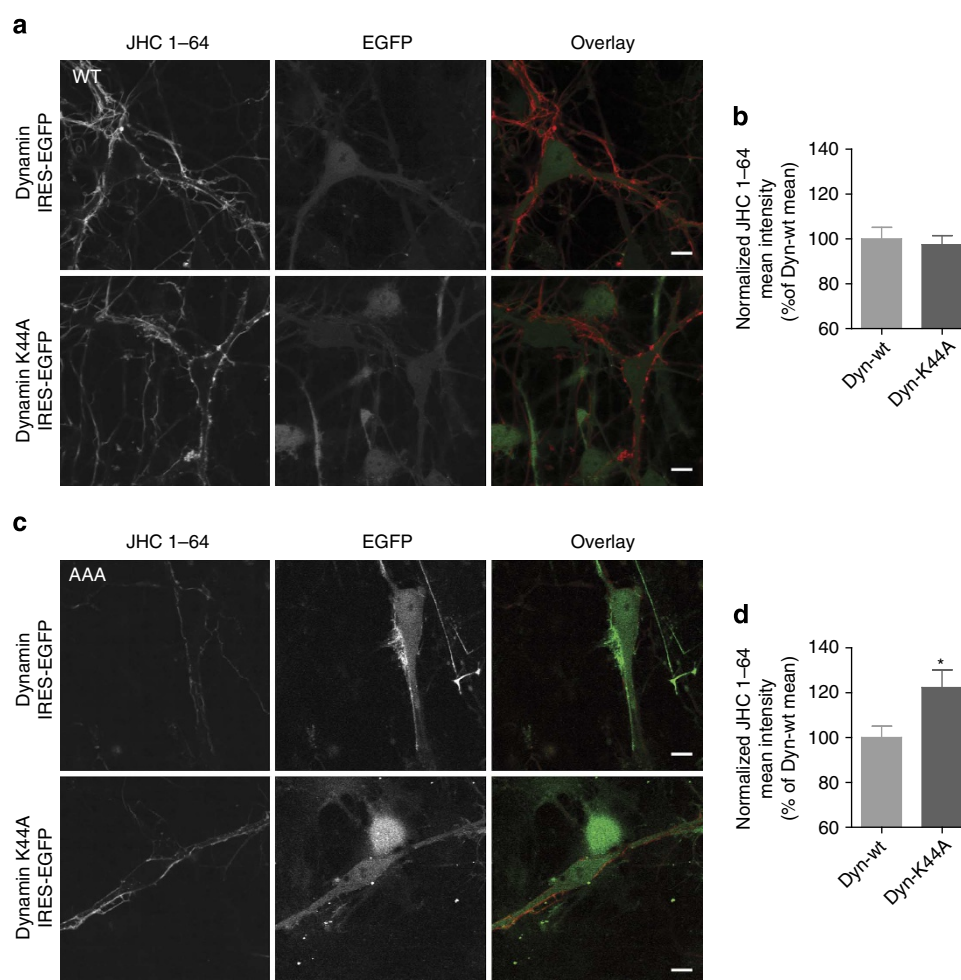

Figure 7 | Inhibition of dynamin-dependent internalization increases surface levels of DAT-AAA, but not WT. (**a**) Midbrain dopaminergic neurons, derived from WT pups, were transduced at day 1–3 *in vitro* with lentivirus encoding either WT dynamin or the dominant-negative K44A dynamin mutant, both coupled to EGFP expression. Left panels, JHC 1–64 labelling (10 nM) of surface-expressed DAT, performed 8–10 days after transduction, to evaluate the effect of inhibiting DAT internalization on surface expression. Middle panels, EGFP signal. Right panels, overlay of channels. (**b**) Quantification of JHC 1–64 fluorescence revealed no difference between WT and K44A dynamin-transduced WT neurons, means ± s.e.m. (n = 34 and 38 neurons for WT dynamin and dynamin-K44A, respectively). (**c**) Midbrain dopaminergic neurons, derived from DAT-AAA pups, transduced with lentivirus encoding either WT dynamin or the dominant-negative K44A dynamin mutant. Left panels, JHC 1–64 labelling (10 nM) of surface-expressed DAT. Middle panels, EGFP signal. Right panels, overlay of channels. (**d**) Inhibition of dynamin-dependent internalization, by dynamin K44A, in DAT-AAA neurons led to a significant increase in the mean JHC 1–64 intensity, relative to control neurons, transduced with WT dynamin (n = 25 and 26 neurons for dynamin WT and K44A respectively, *P < 0.05, non-parametric Mann–Whitney test). Images shown originate from at least five independent stainings from at least four independent neuronal preparations. All images of a given genotype have been taken with identical settings for JHC 1–64 detection. Scale bars, 10 μm.
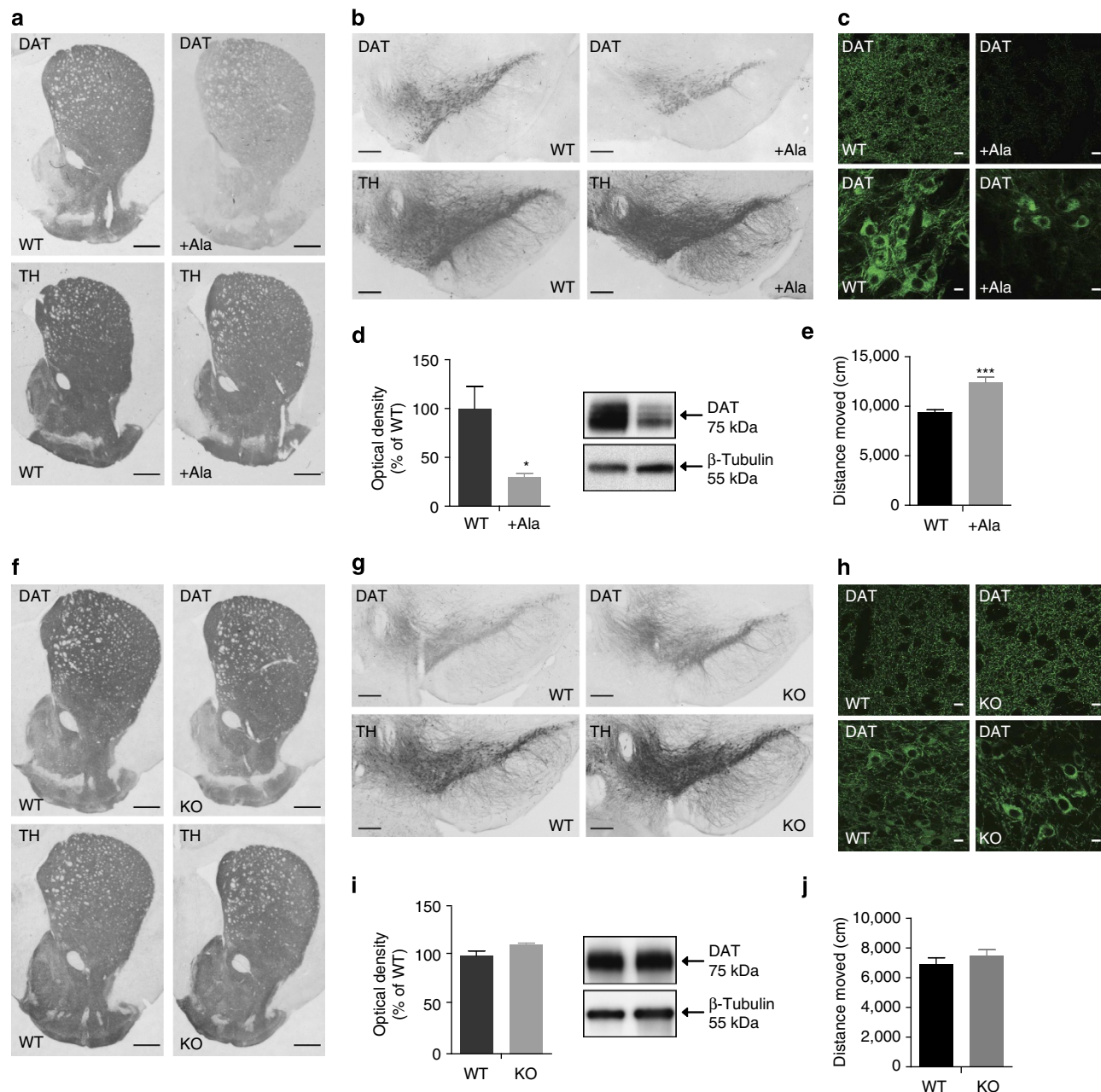
Figure 8 | Immunohistochemical and biochemical characterization of DAT + Ala and PICK1 KO mice. (a,b) Representative photomicrographs of DAT-ir and TH-ir in striatum and midbrain from WT and DAT + Ala mice demonstrate significant loss of DAT-ir in mutant mice, while TH-ir displays similar intensities between both genotypes. **(c)** Upper panels, confocal micrographs of axon terminals in WT and DAT + Ala striatal slices labelled for DAT. Lower panels, DAT labelling in midbrain slices. Both striatum and midbrain show substantial loss of DAT-ir in DAT + Ala mice. Midbrain neurons in WT show extensive DAT labelling in both cell bodies and dendrites, while labelling is reduced and limited to perikarya in DAT + Ala mice. **(d)** Immunoblotting of striatal lysates validates decreased DAT levels in striatum of DAT + Ala. Left panel, densitometric analysis of immunoblots, means ± s.e.m., $n = 4$, *$P < 0.05$, non-parametric Mann–Whitney test. Right panel, representative immunoblots. **(e)** 30 min basal locomotion in the open-field test. Mice were placed in the centre of an open field and locomotion was measured as total distance moved. Data are means ± s.e.m., ***$P < 0.001$, $t(19) = 5.0$; $n_{WT} = 10$, $n_{+Ala} = 11$. **(f,g)** Representative photomicrographs from PICK1 WT and KO mice show intact DAT- and TH-ir in dopaminergic areas in KO mice. **(h)** Upper panels, confocal micrographs of axon terminals in striatal slices from WT and PICK1 KO mice, labelled for DAT. Lower panels, DAT labelling in WT and PICK1 KO midbrain slices. Dense DAT labelling is seen in striatum as well as midbrain of both genotypes. **(i)** Immunoblotting demonstrates similar striatal DAT levels in both WT and PICK1 KO mice. Left panel, densitometric analysis of immunoblots from WT and PICK1 KO mice, means ± s.e.m, $n = 4$, $P > 0.05$, non-parametric Mann–Whitney test. Right panel, representative immunoblots. **(j)** 30 min basal locomotion in the open-field test. Mice were placed in the centre of an open-field and locomotion was measured as total distance moved. Data are means ± s.e.m., $P = 0.34$, $t(44) = 1.0$; $n_{WT} = 27$, $n_{PICK1\ KO} = 19$. Scale bars: **a,f** = 500 µm; **b,g** = 200 µm; **c,h** = 10 µm.

compared with WT (Fig. 8e). To assess whether the phenotype of DAT-AAA and DAT + Ala mice is related to disrupting the interaction with PICK1, we characterized the distribution of

DAT-ir in PICK1 knock-out mice (PICK KO). DAT-ir was not reduced in these mice, neither in the striatum nor in the midbrain. This finding was also validated by immunoblotting (Fig. 8f–i).

Consistently, PICK1 KO mice did not differ from WT in the open-field test (Fig. 8j). Thus, PICK1 is not necessary for axonal distribution of DAT in striatum *in vivo*.

Discussion

To assess the physiological significance of the C-terminal PDZ-binding motif for DAT function *in vivo*, we generated DAT knock-in mice with modified C-termini (DAT-AAA and DAT + Ala) incapable of interacting with PDZ domain proteins. In DAT-AAA, we observed a dramatic reduction in DAT surface levels in striatal presynaptic terminals, likely resulting at least in part from enhanced constitutive endocytosis of the transporter. Moreover, we found that the decreased striatal distribution of DAT leads to unique behavioural changes, characterized by locomotor hyperactivity and impaired amphetamine response. These findings suggest, to our knowledge for the first time, a crucial role of specific protein–protein interactions for synaptic distribution of DAT *in vivo*.

Mutations in proteins often impair folding, leading to ER retention and proteosomal degradation[25]. Indeed, C-terminal truncations have been shown to cause ER retention of human DAT in heterologous cells[8,12,19] and it was suggested that binding of PICK1 to the DAT C-terminus was critical for ER export and DAT surface expression[8]. However, mutational analysis of the human DAT C-terminus showed that, although the C-terminus is critical for proper ER export, PDZ interactions are likely not involved[13]. Our present analysis of mouse DAT-AAA in heterologous cells further corroborated these findings (Supplementary Fig. S3). Furthermore, the present analysis of DAT-AAA and DAT + Ala mice argues against a role of the PDZ-binding motif in ER export *in vivo*, despite the dramatic decrease in striatal DAT levels. It is known that poorly folded and ER-retained DAT mutants give rise to immaturely glycosylated DAT forms sensitive to Endo H[13]. However, for both WT and DAT-AAA mice, we were unable to detect any immaturely glycosylated DAT forms in whole brain extracts, as well as in extracts from cultured dopaminergic neurons. Such forms did not even appear when cultures were treated with the proteosomal inhibitor MG-132 (Supplementary Fig. S2). We believe that DAT-AAA is not ER retained in detectable quantities, but approved by the cellular quality control machinery and allowed to traffic beyond ER.

Previous studies demonstrated that DAT undergoes constitutive and regulated internalization, and that the C-terminal tail might be involved in regulating this trafficking[7,20,26]. We hypothesized accordingly that the observed reduction in synaptic and total DAT-AAA was at least in part the results of decreased surface stability of the transporter and enhanced constitutive endocytosis followed by lysosomal degradation. Importantly, we obtained evidence for a significant increase in constitutive endocytosis of DAT-AAA compared with WTDAT in both striatal slices, using surface biotinylation and in live dopaminergic neurons, using the fluorescent cocaine analogue JHC 1–64 (refs 7,20). Our data also showed that inhibiting constitutive endocytosis by expression of a dominant-negative dynamin mutant K44A, led to partial rescue of DAT-AAA (Figs 6 and 7). No effect was seen for WTDAT possibly because of the much higher expression and thereby different balance between membrane insertion and internalization as compared with DAT-AAA. Finally, we found, in agreement with our previous findings[23], a pronounced co-localization between LysoTracker and internalized WTDAT or DAT-AAA (Fig. 6), supporting that the majority of both internalized DAT and DAT-AAA is sorted to lysosomal degradation[23]. Correspondingly, DAT-AAA and WTDAT co-localized in part with the lysosomal marker LAMP1

in midbrain stainings (Supplementary Fig. S5). Although internalized DAT can undergo recycling[7,20,27], it seems therefore reasonable to suggest that enhanced internalization and subsequent rapid degradation contribute to the DAT-AAA phenotype observed *in vivo* as well as *ex vivo*. Future studies should assess whether additional mechanisms contribute to the observed phenotypes, for example, we cannot exclude that a fraction of synthesized DAT-AAA is missorted and never reaches the presynaptic terminals before it is internalized and degraded in the somatodendritic compartment.

In addition to regulating compartmentalization and targeting[28–30], PDZ domain-mediated protein–protein interactions have previously been suggested to regulate surface stability of membrane proteins[31–33]. Reduced protein expression, but normal synaptic localization, was reported for knock-in mice lacking the PDZ-ligand motif of the metabotropic glutamate receptor mGluR7a, and hypothesized to be caused by increased turnover and degradation, in absence of stabilizing PDZ interactions[34]. It has also been suggested that the postsynaptic scaffolding protein, PSD-95, stabilizes the glycine transporter and the Kv1.4 potassium channel at the plasma membrane[31,33].

PICK1 is the only PDZ domain protein known to bind the DAT C-terminus and the interaction has been addressed in several studies[8,13,14,35]. However, the present data show that the dramatic phenotype observed in both DAT-AAA and DAT + Ala mice is not observed in PICK1 KO mice, arguing that PICK1 is not responsible for maintaining DAT levels in dopaminergic nerve terminals. A remaining challenge is to identify other PDZ domain proteins that bind the DAT C-terminus. A screen of ~40 different PDZ domain including several prototypical synaptic PDZ domain proteins did not identify new DAT-binding partners[36]; hence, further efforts are required to identify potential DAT-binding PDZ domains among an estimated total of 270 PDZ domains in 154 proteins (UniProtKB database). We find it unlikely that the phenotypes of our knock-in mice are the result of disrupting other types of protein–protein interactions because two very different but still PDZ-specific mutations (DAT-AAA/DAT + Ala) result in similar phenotypes. Also note that the binding of Ca^{2+}/calmodulin-dependent protein kinase IIα to the C-terminus of DAT is unaffected by mutation of the PDZ-binding sequence[37].

Our data show that the level of active DAT in DAT-AAA mice is reduced dramatically in the striatum. According to our behavioural analysis, this reduction is accompanied by a hyperactive phenotype when the mice are exposed to a new environment, consistent with increased response to novelty. However, the hyperactivity appears transient as the mice display habituation and show activity indistinguishable from WT after 2 h. This is in contrast to DAT KO mice that show only modest habituation even after several hours[5]. In further contrast, DAT-AAA mice show less pronounced adaptive changes, as TH expression is essentially unaltered in DAT-AAA, whereas TH levels are reduced by 90% in DAT KO[38]. In addition, DAT-AAA mice show no growth retardation phenotype (Supplementary Table S1). Together, our data imply that the function of the residual transporters in DAT-AAA is sufficient for maintaining a 'closer to normal' homoeostasis within the dopaminergic system. It is also interesting to compare the DAT-AAA mice with DAT-knock-down (DAT KD) mice expressing ~10% of WT DAT levels[39]. DAT KD mice are hyperactive upon exposure to a novel environment and characterized by an equivalent modest habituation deficit similar to DAT-AAA and show no sign of endocrine deficits[39]. However, DAT KD and DAT-AAA mice show a difference in their response to amphetamine. Whereas amphetamine fails to induce hyperlocomotion in DAT-AAA mice, it inhibits locomotor activity in DAT KD mice similar to

what is seen in DAT KO mice[39]. We have no immediate explanation for the differential effect of amphetamine. However, whereas the reduced DAT levels in DAT KD mice are caused by defective transcription[39], the DAT-AAA phenotype is related to changed turnover of translated protein, which may have differential functional consequences.

Summarized, we have generated two new mouse DAT models that together strongly support an indispensable role of a C-terminal PDZ-binding sequence *in vivo*. Furthermore, these two new mouse models are characterized by unique dopaminergic phenotypes and represent thereby novels tools for further dissecting the relationship between dopaminergic dysfunction and CNS disorders.

Methods

Site-directed mutagenesis. Constructs were generated as described in Supplementary Methods.

Fluorescence polarization assay. Experiments were performed as previously described[14].

Mouse genetics. Mutant alleles with modified C-termini were generated in CJ7 ES cells using the knock-in approach[40] as described (Supplementary Methods, Supplementary Figs S1 and S5). The PICK1-deficient mice were kindly provided by Dr Richard Huganir (Johns Hopkins University, Baltimore, USA). All mice experiments were performed in accordance with guidelines of the Danish Animal Experimentation Inspectorate (permission number: 2012/561-142).

Quantitative real-time PCR. Assay was carried out as described in Supplementary Methods.

Immunohistochemistry. Adult mice were transcardially perfused with 4% paraformaldehyde in 0.1 M PBS pH 7.4. Coronal and sagittal sections (40 μm) were generated from striatum and midbrain. For bright-field immunohistochemistry, a standard peroxidase-based method using 3,3′-diaminobenzidine was used as previously described[41]. The following primary antibodies were used: rat anti-DAT antibody (MAB369 1:1,000, Millipore, USA) or rabbit polyclonal anti-TH antibody (1:1,000, Affinity Bioreagents, USA).

Co-localization studies of DAT-ir neurons were performed using dual-labelling immunofluorescence. Sections were incubated overnight with rat anti-DAT antibody (1:1,000) and either rabbit anti-TH antibody (1:1,000) or rabbit polyclonal LAMP1 (1:200, Abcam). The following day sections were rinsed and incubated with Alexa Fluor 488 goat anti-rat IgG (for DAT) and Alexa Fluor 568 goat anti-rabbit IgG (for TH and LAMP1) conjugated secondary antibodies for 1 h (Molecular Probes, USA). Additional rinsing was followed by mounting of coverslips using Prolong Gold antifade reagent (Molecular Probes, USA).

Confocal microscopy. Confocal microscopy was performed as described[18,23], using a Zeiss (Carl Zeiss, Germany) LSM 510 confocal laser-scanning microscope with an oil immersion 63 × 1.4 numerical aperture objective (Carl Zeiss). Alexa Fluor 488 dye was excited with a 488-nm laserline from an argon-krypton laser, and detection of the emitted light was done using a 505- to 530-nm bandpass filter. Alexa Fluor 568 dye and JHC 1–64 were excited with a 543-nm helium-neon laser and fluorescence was recorded using a 560-nm long-pass filter. Images were analysed with ImageJ software.

Quantification of optical density. Optical densitometry was applied for semi-quantification of DAT and TH immunoreactivity and performed as described in Supplementary Methods.

Glial coating. Astrocytes cultures from mouse cortex were made and maintained as previously described[42]. 5-fluorodeoxyuridine was added, when density reached 70%, approximately after 5 days.

Primary cultures of midbrain dopaminergic neurons. Postnatal dopaminergic neurons from WT and DAT-AAA mice were obtained and cultured as described[18]. Neurons were plated on glial-coated coverslips (∼200,000 cells per slide) for immunocytochemistry and in glial-coated 2-well LabTek chambers for live imaging (∼100,000 cells per well). Experiments were performed after culturing 7–14 days *in vitro*.

Immunocytochemistry. Dopaminergic neurons, grown on glia-coated coverslips, were treated as described[43], though permebilization was done in PBS containing 5% goat serum and 0.2% saponin for 20 min. Primary rat anti-DAT antibody (MAB369 1:1,000) and secondary Alexa Fluor 488 (goat anti-rat IgG) (1:500) were used to visualize DAT.

Lentivirus production and transduction. Lentiviral vectors encoding GFP-tagged WT and dominant-negative (K44A) dynamin (pFUGW-IRES-GFP Dynamin K44A or pFUGW-IRES-GFP Dynamin) were kindly provided by Dr Rosalind A Segal (Harvard Medical School, Boston, MA), and produced as described[18]. Dopaminergic neurons were transduced at day 1–3 *in vitro* and experiments were performed 7–10 days after infection.

Live imaging of dopaminergic neurons. Surface-expressed DAT was visualized in live ventral midbrain dopaminergic neurons, transduced as well as untransduced, as described[18], using 10 nM JHC1–64 for 20 min at room temperature to stain DAT.

The effect of inhibiting dynamin-dependent endocytosis on DAT surface levels was evaluated by quantifying mean JHC 1–64 labelling intensity of WT and DAT-AAA neurons, transduced with pFUGW-IRES-GFP Dynamin K44A or pFUGW-IRES-GFP WT Dynamin as control. Transduced neurons were identified from the coupled EGFP expression. Excitation and recording of JHC 1–64 fluorescence (see 'confocal microscopy') was carried out using identical settings for all pictures taken of a given genotype, but differences in expression made it necessary to use different settings for WT and DAT-AAA neurons. A region of interest (ROI), containing the neuronal soma and proximal extensions, was manually selected on single confocal sections. The mean intensity of JHC 1–64 labelling within this ROI was quantified as the mean pixel intensity divided by the area percentage with JHC 1–64 signal, using the same threshold for all images of a given genotype.

Internalization of DAT in live WT and DAT-AAA neurons was assessed as described[18], using 10 nM JHC 1–64 to label surface DAT at 4 °C before 1 h internalization at 37 °C (or 4 °C as a temperature control). The neuronal soma and proximal extensions was manually selected on single confocal sections (ROI-total). The cytoplasmic region of ROI-total (that is, excluding the plasma membrane) was subsequently manually defined (ROI-internalized). Threshold was set as twice the mean intensity within ROI-total, to ensure that only specific JHC 1–64 signal contributed to the quantification. The total integrated JHC 1–64 intensity within ROI-total was taken as a measure of the entire labelled DAT pool, while the total integrated JHC 1–64 intensity within ROI-internalized was taken as a measure of internalized DAT/JHC 1–64. The internalized fraction of DAT/JHC 1–64 complexes was obtained as the ratio between the internalized JHC 1–64 and the total JHC 1–64. Of notice, differences in expression made it necessary to use images taken with different settings for quantification of WT and DAT-AAA internalization.

For LysoTracker co-localization studies, internalized DAT was visualized as described above, adding LysoTracker green (100 nM; Molecular Probes) in the last 15 min of incubation to visualize lysosomes. Neurons were washed twice in uptake buffer before imaging.

Membrane and whole-cell lysate preparations. Preparation of membrane fractions from adult mice striata and whole pup brains is described in Supplementary Methods, along with the preparation of whole-cell lysates from adult mice striata (for estimations of total TH expression) and whole-cell lysates from cultured dopaminergic neurons.

Brain slice preparation and surface biotinylation. Experiments were performed as described in Supplementary Methods, modified from ref. 44.

Immunoblotting. Immunoblotting was performed as described in Supplementary Methods.

Dopamine uptake *in vitro*. Uptake experiments were performed as described in Supplementary Methods.

Striatal membrane binding assay. Competition binding assays were performed on striatal membrane preparations, using the DAT ligand, [125I]-RTI-55 (2,200 Ci per mmol, Perkin Elmer, USA). Membrane suspensions were mixed with ∼1 nM [^{125}I]-RTI-55 in a total volume of 500 μl and samples were incubated in binding buffer containing 25 mM HEPES pH 7.4, 120 mM NaCl, 5 mM KCl, 1.2 mM CaCl$_2$, 1.2 mM MgSO$_4$ for 2 h at 4 °C with constant shaking. To avoid unspecific binding of RTI-55 to the serotonin and norepinephrine transporters, 50 nM s-citalopram and 100 nM desipramine were included. The assay was terminated with ice-cold binding buffer, followed by loading of membranes on glass microfiber filters (GF/C Whatman). Filters were rinsed in ice-cold binding buffer and allowed to dry before scintillation fluid was added and samples were counted 1 h thereafter. Non-specific binding was assessed in the presence of 1 mM

dopamine. Binding data were analysed by non-linear regression analysis assuming one-site binding (GraphPad Prism 5.0).

Autoradiography. Assay was performed as described in Supplementary Methods.

Synaptosomal dopamine uptake. Striata were dissected out from coronal slices and homogenized in ice-cold HEPES buffer (4 mM, pH = 7.4) containing 0.32 M sucrose. Crude synaptosome fraction (P2) was obtained as described in membrane preparations (Supplementary Methods) and dopamine uptake was performed with minor modifications[45]. Unlabelled dopamine (0.125 µM) was added together with [3H]-Dopamine (Perkin Elmer Life Sciences, USA) for assessment of dopamine uptake for 5 min at 37 °C. Uptake was terminated by addition of ice-cold uptake buffer. Non-specific uptake was determined in the presence of 100 µM cocaine. Synaptosomes were loaded on glass microfiber filters (GF/C Whatman), rinsed 4 × 5 ml in uptake buffer and allowed to air-dry. Scintillation fluid was added and filters were agitated for 1 h followed by counting.

Behavioural phenotype assessment (SHIRPA). Behavioural and physical characteristics of experimentally naive mice were assessed using the SHIRPA primary screen procedure as described[17].

Basal locomotion and amphetamine-induced hyperactivity. Using a previously described set-up[46], three experiments were carried out. (1) Basal locomotor activity: the animal was placed in an activity box and the activity measured for 4 h; (2) 1 h amphetamine-induced hyperactivity after i.p. injection of amphetamine (1–3 mg kg^{-1}) or saline; (3) amphetamine-induced hyperactivity (2 mg kg^{-1} i.p.) for 2.5 h after habituation to the activity boxes for 2.5 h. Furthermore, basal locomotion of DAT-AAA, DAT + Ala KI and PICK1 KO mice and WT littermates was investigated in an open-field test. The animals were placed individually in the centre of an open field (40 × 40 × 65 cm), illuminated indirectly by four 60-W white light bulbs, and allowed to explore the apparatus for 30 min (ref. 46). Behaviour was recorded with a camera mounted on the ceiling directly above the open field and total distance moved was analysed using EthoVision Software (version 3.0; Noldus, The Netherlands).

Statistics. Unless otherwise stated Mann–Whitney non-parametric test was applied. One- or two-way analysis of variance, followed by Bonferroni *post-hoc* *t*-tests or Kruskal–Wallis non-parametric test, were applied when comparing more than two groups. Significance level was set at $P < 0.05$.

References

1. Kristensen, A. S. *et al.* SLC6 neurotransmitter transporters: structure, function, and regulation. *Pharmacol. Rev.* **63**, 585–640 (2011).
2. Gainetdinov, R. R. & Caron, M. G. Monoamine transporters: from genes to behavior. *Annu. Rev. Pharmacol. Toxicol.* **43**, 261–284 (2003).
3. Torres, G. E. & Amara, S. G. Glutamate and monoamine transporters: new visions of form and function. *Curr. Opin. Neurobiol.* **17**, 304–312 (2007).
4. Sulzer, D., Sonders, M. S., Poulsen, N. W. & Galli, A. Mechanisms of neurotransmitter release by amphetamines: a review. *Prog. Neurobiol.* **75**, 406–433 (2005).
5. Giros, B., Jaber, M., Jones, S. R., Wightman, R. M. & Caron, M. G. Hyperlocomotion and indifference to cocaine and amphetamine in mice lacking the dopamine transporter. *Nature* **379**, 606–612 (1996).
6. Bosse, R. *et al.* Anterior pituitary hypoplasia and dwarfism in mice lacking the dopamine transporter. *Neuron* **19**, 127–138 (1997).
7. Eriksen, J., Jorgensen, T. N. & Gether, U. Regulation of dopamine transporter function by protein-protein interactions: new discoveries and methodological challenges. *J. Neurochem.* **113**, 27–41 (2010).
8. Torres, G. E. *et al.* Functional interaction between monoamine plasma membrane transporters and the synaptic PDZ domain-containing protein PICK1. *Neuron* **30**, 121–134 (2001).
9. Standley, S., Roche, K. W., McCallum, J., Sans, N. & Wenthold, R. J. PDZ domain suppression of an ER retention signal in NMDA receptor NR1 splice variants. *Neuron* **28**, 887–898 (2000).
10. Armsen, W., Himmel, B., Betz, H. & Eulenburg, V. The C-terminal PDZ-ligand motif of the neuronal glycine transporter GlyT2 is required for efficient synaptic localization. *Mol. Cell Neurosci.* **36**, 369–380 (2007).
11. Kim, E. & Sheng, M. PDZ domain proteins of synapses. *Nat. Rev. Neurosci.* **5**, 771–781 (2004).
12. Torres, G. E. *et al.* Oligomerization and trafficking of the human dopamine transporter. Mutational analysis identifies critical domains important for the functional expression of the transporter. *J. Biol. Chem.* **278**, 2731–2739 (2003).
13. Bjerggaard, C. *et al.* Surface targeting of the dopamine transporter involves discrete epitopes in the distal C terminus but does not require canonical PDZ domain interactions. *J. Neurosci.* **24**, 7024–7036 (2004).
14. Madsen, K. L. *et al.* Molecular determinants for the complex binding specificity of the PDZ domain in PICK1. *J. Biol. Chem.* **280**, 20539–20548 (2005).
15. Ciliax, B. J. *et al.* The dopamine transporter: immunochemical characterization and localization in brain. *J. Neurosci.* **15**, 1714–1723 (1995).
16. Hersch, S. M., Yi, H., Heilman, C. J., Edwards, R. H. & Levey, A. I. Subcellular localization and molecular topology of the dopamine transporter in the striatum and substantia nigra. *J. Comp. Neurol.* **388**, 211–227 (1997).
17. Schmidt, L. S. *et al.* Increased cocaine self-administration in M4 muscarinic acetylcholine receptor knockout mice. *Psychopharmacology (Berl)* **216**, 367–378 (2011).
18. Eriksen, J. *et al.* Visualization of dopamine transporter trafficking in live neurons by use of fluorescent cocaine analogs. *J. Neurosci.* **29**, 6794–6808 (2009).
19. Sorkina, T., Doolen, S., Galperin, E., Zahniser, N. R. & Sorkin, A. Oligomerization of dopamine transporters visualized in living cells by fluorescence resonance energy transfer microscopy. *J. Biol. Chem.* **278**, 28274–28283 (2003).
20. Sorkina, T., Hoover, B. R., Zahniser, N. R. & Sorkin, A. Constitutive and protein kinase C-induced internalization of the dopamine transporter is mediated by a clathrin-dependent mechanism. *Traffic* **6**, 157–170 (2005).
21. Chi, L. & Reith, M. E. Substrate-induced trafficking of the dopamine transporter in heterologously expressing cells and in rat striatal synaptosomal preparations. *J. Pharmacol. Exp. Ther.* **307**, 729–736 (2003).
22. Holton, K. L., Loder, M. K. & Melikian, H. E. Nonclassical, distinct endocytic signals dictate constitutive and PKC-regulated neurotransmitter transporter internalization. *Nat. Neurosci.* **8**, 881–888 (2005).
23. Eriksen, J., Bjorn-Yoshimoto, W. E., Jorgensen, T. N., Newman, A. H. & Gether, U. Postendocytic sorting of constitutively internalized dopamine transporter in cell lines and dopaminergic neurons. *J. Biol. Chem.* **285**, 27289–27301 (2010).
24. van der Bliek, A. M. *et al.* Mutations in human dynamin block an intermediate stage in coated vesicle formation. *J. Cell Biol.* **122**, 553–563 (1993).
25. Ellgaard, L. & Helenius, A. Quality control in the endoplasmic reticulum. *Nat. Rev. Mol. Cell Biol.* **4**, 181–191 (2003).
26. Sakrikar, D. *et al.* Attention deficit/hyperactivity disorder-derived coding variation in the dopamine transporter disrupts microdomain targeting and trafficking regulation. *J. Neurosci.* **32**, 5385–5397 (2012).
27. Rao, A., Simmons, D. & Sorkin, A. Differential subcellular distribution of endosomal compartments and the dopamine transporter in dopaminergic neurons. *Mol. Cell Neurosci.* **46**, 148–158 (2011).
28. Perego, C. *et al.* PDZ-mediated interactions retain the epithelial GABA transporter on the basolateral surface of polarized epithelial cells. *EMBO J.* **18**, 2384–2393 (1999).
29. Fairless, R. *et al.* Polarized targeting of neurexins to synapses is regulated by their C-terminal sequences. *J. Neurosci.* **28**, 12969–12981 (2008).
30. Farhan, H. *et al.* Two discontinuous segments in the carboxyl terminus are required for membrane targeting of the rat gamma-aminobutyric acid transporter-1 (GAT1). *J. Biol. Chem.* **279**, 28553–28563 (2004).
31. Cubelos, B., Gonzalez-Gonzalez, I. M., Gimenez, C. & Zafra, F. The scaffolding protein PSD-95 interacts with the glycine transporter GLYT1 and impairs its internalization. *J. Neurochem.* **95**, 1047–1058 (2005).
32. D'Amico, A. *et al.* The surface density of the glutamate transporter EAAC1 is controlled by interactions with PDZK1 and AP2 adaptor complexes. *Traffic* **11**, 1455–1470 (2010).
33. Jugloff, D. G., Khanna, R., Schlichter, L. C. & Jones, O. T. Internalization of the Kv1.4 potassium channel is suppressed by clustering interactions with PSD-95. *J. Biol. Chem.* **275**, 1357–1364 (2000).
34. Zhang, C. S. *et al.* Knock-in mice lacking the PDZ-ligand motif of mGluR7a show impaired PKC-dependent autoinhibition of glutamate release, spatial working memory deficits, and increased susceptibility to pentylenetetrazol. *J. Neurosci.* **28**, 8604–8614 (2008).
35. Madsen, K. L., Thorsen, T. S., Rahbek-Clemmensen, T., Eriksen, J. & Gether, U. Protein interacting with C kinase 1 (PICK1) reduces reinsertion rates of interaction partners sorted to the RAB11-dependent slow recycling pathway. *J. Biol. Chem.* **287**, 12293–12308 (2012).
36. Ratjhe, M. A. *et al.* A PDZ domain library: investigating specificity of PDZ domain small-molecule inhibitors. *Program No. 850.18. 2010 Neuroscience Meeting Planner* (San Diego, CA: Society for Neuroscience, 2010. Online).
37. Fog, J. U. *et al.* Calmodulin kinase II interacts with the dopamine transporter C terminus to regulate amphetamine-induced reverse transport. *Neuron* **51**, 417–429 (2006).
38. Jaber, M. *et al.* Differential regulation of tyrosine hydroxylase in the basal ganglia of mice lacking the dopamine transporter. *Eur. J. Neurosci.* **11**, 3499–3511 (1999).
39. Zhuang, X. *et al.* Hyperactivity and impaired response habituation in hyperdopaminergic mice. *Proc. Natl Acad. Sci. USA* **98**, 1982–1987 (2001).

40. Swiatek, P. J. & Gridley, T. Perinatal lethality and defects in hindbrain development in mice homozygous for a targeted mutation of the zinc finger gene Krox20. *Genes Dev.* **7,** 2071–2084 (1993).

41. Rickhag, M., Deierborg, T., Patel, S., Ruscher, K. & Wieloch, T. Apolipoprotein D is elevated in oligodendrocytes in the peri-infarct region after experimental stroke: influence of enriched environment. *J. Cereb. Blood Flow Metab.* **28,** 551–562 (2008).

42. Biber, K., Klotz, K. N., Berger, M., Gebicke-Harter, P. J. & van Calker, D. Adenosine A1 receptor-mediated activation of phospholipase C in cultured astrocytes depends on the level of receptor expression. *J. Neurosci.* **17,** 4956–4964 (1997).

43. Madsen, K. L. *et al.* Membrane localization is critical for activation of the PICK1 BAR domain. *Traffic* **9,** 1327–1343 (2008).

44. Thomas-Crusells, J., Vieira, A., Saarma, M. & Rivera, C. A novel method for monitoring surface membrane trafficking on hippocampal acute slice preparation. *J. Neurosci. Methods* **125,** 159–166 (2003).

45. Richards, T. L. & Zahniser, N. R. Rapid substrate-induced down-regulation in function and surface localization of dopamine transporters: rat dorsal striatum versus nucleus accumbens. *J. Neurochem.* **108,** 1575–1584 (2009).

46. Sorensen, G. *et al.* Neuropeptide Y Y5 receptor antagonism attenuates cocaine-induced effects in mice. *Psychopharmacology (Berl)* **222,** 565–577 (2012).

Acknowledgements

Author contributions

M.R., F.H.H., G.S., K.N.S., B.A., K.G., K.L.M. and I.V.K. conducted the experiments. I.A.-J., J.E., G.W. and D.P.D.W. provided scientific input. K.N.S., E.-M.F. and J.G. generated knock-in mice. A.H.N. provided the fluorescent cocaine analogue JHC 1–64. M.R., F.H.H., G.S., K.N.S. and U.G. designed the experiments and evaluated the data. M.R., F.H.H., G.S. and U.G. wrote the manuscript.

Additional information

Supplementary Information accompanies this paper at http://www.nature.com/naturecommunications

Competing financial interests: The authors declare no competing financial interests.

Reprints and permission information is available online at http://npg.nature.com/reprintsandpermissions/

How to cite this article: Rickhag, M. *et al.* A C-terminal PDZ domain-binding sequence is required for striatal distribution of the dopamine transporter. *Nat. Commun.* 4:1580 doi: 10.1038/ncomms2568 (2013).

Corrigendum: A C-terminal PDZ domain-binding sequence is required for striatal distribution of the dopamine transporter

Mattias Rickhag, Freja Herborg Hansen, Gunnar Sørensen, Kristine Nørgaard Strandfelt, Bjørn Andresen, Kamil Gotfryd, Kenneth L. Madsen, Ib Vestergaard Klewe, Ina Ammendrup-Johnsen, Jacob Eriksen, Amy H. Newman, Ernst-Martin Füchtbauer, Jesus Gomeza, David P.D. Woldbye, Gitta Wörtwein & Ulrik Gether

The original version of this Article contained an error in the spelling of the author Ib Vestergaard Klewe, which was incorrectly given as Ib Vestergaard-Klewe. This has now been corrected in both the PDF and HTML versions of the Article.